JACS
JOURNAL OF THE AMERICAN CHEMICAL SOCIETY

Article

pubs.acs.org/JACS

Laser-Induced Explosion of Nitrated Carbon Nanotubes: Nonadiabatic and Reactive Molecular Dynamics Simulations

Vitaly V. Chaban,[†] Sougata Pal,[‡] and Oleg V. Prezhdo*[,‡]

[†]Instituto de Ciência e Tecnologia, Universidade Federal de São Paulo, São José dos Campos, 12231-280 São Paulo, Brazil
[‡]Department of Chemistry, University of Southern California, Los Angeles, California 90089, United States

Supporting Information

ABSTRACT: Laser-initiated decomposition of carbon nanotubes (CNTs) can lead to medical, military, and other applications. In medicine, CNTs give rise to efficient remedies against diseases and malignant cells, since they encapsulate drug molecules, can be delivered inside living organisms, and absorb light that penetrates through biological tissues. As explosives, pyrotechnics, and propellants, CNTs can be activated remotely by a visible or infrared laser, avoiding the need for a detonating cord. The reported non-equilibrium investigation demonstrates the possibility of photoinduced polynitro-CNT explosion and provides a detailed chemical mechanism of the decomposition process, explicitly in the time domain. Nonadiabatic molecular dynamics (MD) performed with real-time time-dependent tight-binding density functional theory demonstrates that the photogenerated exciton deposits its energy into a broad range of phonon modes within less than a picosecond, resulting in a rapid polynitro-CNT heating. Following the heating, reactive MD demonstrates an explosion, during which the local temperature of polynitro-CNTs and its fragments rises as high as 4000 K. Photoexcitation of nitro groups by a high-energy laser is not required; the energy can be delivered to polynitro-CNTs using near-infrared light within the biological window. Furthermore, the explosion is possible both with and without an external oxygen source. Anaerobic explosion could be particularly beneficial in confined biological and nanoscale environments. The products of the polynitro-CNT decomposition are nontoxic: carbon dioxide and molecular nitrogen. The in silico demonstration of the laser-induced polynitro-CNT explosion, its chemical mechanism, and the time scales of physical and chemical transformations can be tested experimentally using time-resolved laser techniques.

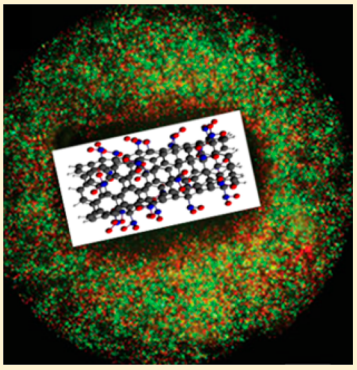

1. INTRODUCTION

The unique properties of carbon nanotubes (CNTs) give rise to multiple applications in a variety of fields. In addition to materials science,[1−14] CNTs draw interest in a new generation of medical applications.[15−23] For instance, CNTs are widely functionalized with biologically relevant molecules to work as cancer treatment and drug delivery systems, and bio-markers.[15,16,18,19,22−26] Nanoscale drug delivery vehicles possess versatile imaging, diagnostic, and therapeutic characteristics. They hold promise for fighting diseases of various types, including cancer, infections, and neurodegenerative syndromes. Laser-initiated release of molecules carried by CNTs can be made very localized within a body, allowing for focused treatments and eliminating broad damage of surrounding tissues, which is unavoidable, for instance, with chemo-therapy. In an entirely different direction, laser-initiated decomposition of the appropriately functionalized CNTs can give rise to a novel class of high-energy nanomaterials, eliminating the needs for a detonation cord.[27] The potential applications of nanoscale explosives extend beyond military, civil, and industrial purposes.[28−32]

There is sufficient evidence in literature that CNTs can exhibit cytotoxic properties.[33,34] Multiwalled CNTs resemble microtubules in many aspects. They enter inside living cells and form mixed biosynthetic polymers with tubulin. Such polymers strongly interfere with biomechanical processes in the living cell and eventually kill proliferating cells, acting as conventional microtubule stabilizing drugs. Pristine multiwalled CNTs can be used to kill cancer cells without the need to perform their functionalization.[35]

CNTs provide new opportunities for encapsulation and targeted delivery of drugs.[16−18,20,23] Normally, efficacy of drugs is decreased if no carrier is used, in particular since most drug molecules are polar and cannot penetrate through hydrophobic cell membranes. The ability of drugs to reach a target site depends on their physical-chemical properties. Intracellular transport of drugs, genes, and proteins is becoming feasible as a result of the recent technical advances in chemical synthesis.[24−26] In the case of nanoscale carriers, the drug delivery formulations transport drugs selectively to specific compartments, to avoid adverse effects on surrounding tissues. The most actively probed nanoscale drug carriers are built on self-assembling polymeric structures, mesoporous silica, magnetic nanoparticles (e.g., Fe_3O_4), and CNTs.[25,26]

Received: August 3, 2016
Published: November 19, 2016

DOI: 10.1021/jacs.6b08082
J. Am. Chem. Soc. 2016, 138, 15927−15934

Noninvasive activation of CNTs can be achieved by a laser emitting near-infrared light. These wavelengths pass through living tissues, while they are absorbed by CNTs.[35] Most energy of the adsorbed light goes to excite electrons. Then, the energy transfers to phonons as a result of electron−phonon relaxation. Thus, CNTs can be quickly and safely heated up by remote means.

CNTs are highly hydrophobic. It is impossible to solubilize pristine CNTs in aqueous solutions. Surface functionalization can increase solubility and biocompatibility.[25,33] Two different types of CNT functionalization exist: covalent binding of functional groups using a carbon-based chemical reaction and noncovalent functionalization. In the latter case, hydrophobic interactions are employed to keep the resulting complex as a whole. Grafting nitro ($-NO_2$) groups increases solubility of the initially strongly hydrophobic CNTs. For comparison, nitromethane is very well miscible with water,[36] while solubility of methane is mediocre.

Nitro groups are widely used in explosive materials due to their high energetic content and strong oxidizing properties. $-NO_2$ provides significant amounts of oxygen, enabling full or partial oxidation of chemical species and contributing strongly to detonation and combustion processes. Chemical methods have proven to be very effective in changing the properties of nanoscale carbon materials.[37,38] It is chemically straightforward to obtain nitrated derivatives of nanoscale carbon. Nitration promotes fast exothermic decomposition upon initial heating, as demonstrated by the recent simulations.[36,39] Synthesis of polynitrofullerenes has been reported recently.[40,41] As stable molecules with a high energy of formation, polynitrofullerenes can explode under certain conditions, as demonstrated by the real-time constant-energy simulation.[42]

Polynitro-CNTs are advantageous to fullerenes, since they absorb visible and infrared light and their explosion can therefore be initiated by readily available lasers. The unique combination of CNT's chemical and physical principles can lead to significant advances in energetic nanomaterials. Nanoscale explosives constitute a novel and rapidly developing field, requiring development of more efficient and less toxic materials. Carbon-based nanomaterials exhibit structural diversity[43] and provide an exceptional platform for the development and research of reactive energetic systems.

The present work focuses on single-walled CNTs with external surfaces functionalized by multiple nitro groups and demonstrates that a remote activation by a laser leads to their rapid decomposition. We report nonadiabatic simulation of the electron−phonon relaxation, followed by reactive simulation of the CNT decomposition. The two-step investigation of the photoinduced polynitro-CNT explosion provides a detailed chemical mechanism of the decomposition process. Time-dependent tight-binding density functional theory (DFT), combined with nonadiabatic molecular dynamics (MD), demonstrates that the photogenerated charge carriers rapidly lose their energy to heat. As demonstrated by reactive MD, the heating initiates an explosion, during which the temperature rises to as high as 4000 K. Importantly, the explosion is possible both with and without an external oxygen source, although extra oxygen helps to release more energy. The simulations establish the mechanisms and time scales of chemical and physical transformations. The predictions can be tested experimentally using time-resolved laser techniques.

2. SIMULATION METHODOLOGIES

The simulations are performed using a combination of two MD techniques, designed to capture the two sequential steps of the photoinduced explosion of polynitro-CNTs. The first step, involving laser excitation of CNT's electronic subsystem and electron−phonon energy redistribution is modeled by nonadiabatic (NA) MD that is capable of describing quantum transitions down the manifold of CNT electronic states. Here, the CNT electronic properties are described using tight-binding density functional theory (DFTB), which is parametrized against ab initio DFT calculations. The second step, involving chemical decomposition of polynitro-CNTs, is 2 orders of magnitude slower. It is modeled using reactive MD (RMD), which employs classical reactive force fields (ReaxFF) that are also parametrized using ab initio DFT and other quantum−chemical methods. DFTB-NAMD allows simulations up to several picoseconds, which is more than sufficient to study the electron−phonon energy redistribution, but is too short to observe the full mechanism of nitro-CNT decomposition. RMD simulations can be performed over hundreds of picoseconds, allowing us to simulate complete polynitro-CNT destruction and to study its chemical mechanism.

2.1. Nonadiabatic Molecular Dynamics. Modeling of laser-induced electronic excitation and subsequent nonradiative electron-vibrational relaxation requires an explicit treatment of electronic degrees of freedom, electron-vibrational coupling, and transitions between electronic states caused by coupling to vibrations. This goal is achieved using the recently developed methodology[44] that combines NAMD with DFTB. The evolution of the electronic subsystem driven by vibrational motions is described with self-consistent charge DFTB (SCC-DFTB),[45−51] available at www.dftb-plus.info, with parameters sets provided at www.dftb.org. The NAMD simulation is performed in the Kohn−Sham (KS) representation,[52−54] using the fewest switching surface hopping (FSSH) technique[55,56] as implemented in the PYXAID (Python eXtension for Ab Initio Dynamics) code,[57,58] available at www.acsu.buffalo.edu/~alexeyak/pyxaid/. The electrons are treated quantum−mechanically, while the nuclei are treated classically.[59] The simulations are performed in the adiabatic representation, in which the electronic structure calculation method produces both the energy levels and NA couplings between the states for current nuclear positions.

All quantum−mechanical calculations including geometry optimization, electronic structure, and adiabatic MD are carried out with the SCC-DFTB method[45−51] as implemented in the DFTB+ code.[45,60] The simulations are performed using periodic boundary conditions. The simulation cell constant is fully optimized in the z-direction along the CNT axis; 40 Å of vacuum is added in the x- and y-directions, in order to avoid interactions between the polynitro-CNT periodic replicas, since the focus is on single-walled CNTs. The optimized cell lengths in the z-direction are 21.50 and 17.29 Å for the (5,0) and (5,5) polynitro-CNTs, respectively. The diameters of the optimized polynitro-CNTs are 3.94 Å for the (5,0) CNT and 6.80 Å for the (5,5) polynitro-CNT. The total number of carbon atoms in the simulation cell is 100 and 140 for the (5,0) and (5,5) polynitro-CNTs, respectively. The total number of $-NO_2$ groups functionalizing the two CNTs is chosen to maintain the carbon/nitrogen atom ratio at 5:1.

The SSC-DFTB parameter set (Slater-Koster files) used in the calculations was tested extensively for a broad range of

DOI: 10.1021/jacs.6b08082
J. Am. Chem. Soc. 2016, 138, 15927−15934

compounds and can be found elsewhere.[47] The density of states (DOS) was computed using a 1 × 1 × 256 Monkhorst−Pack *k*-point mesh.[61] Starting with the optimized geometries, the polynitro-CNTs were heated to 300 K with repeated velocity rescaling. Then, 3 ps microcanonical trajectory was generated for each polynitro-CNT in the ground electronic state, using the Verlet algorithm[62] with the 1 fs time step and Hellman-Feynman forces. Five-hundred geometries were saved based on the 2 ps long microcanonical trajectory for each CNT to perform NAMD. Optically active electron and hole states with energies around 1 eV away from the Fermi energy were selected to initiate the coupled electron electron-vibrational evolution. Several hundred iterations of the stochastic FSSH algorithm were used to achieve converged results. Further details of the NAMD methodology are given elsewhere.[53,57,58]

2.2. Reactive Molecular Dynamics. RMD simulations were used to observe decomposition of the (5,0) and (5,5) polynitro-CNTs in real-time. ReaxFFs[63,64] allow one to avoid costly quantum−chemical description of the simulated system by introducing a set of sophisticated interaction potentials. Covalent bonds in RMD emerge and break apart during the simulation based on the value of the bond-order parameter. ReaxFFs are normally parametrized by means of multiple single-point DFT calculations involving expected reactants, intermediates, and products. The ReaxFF applied in our present study has been carefully developed for carbon, hydrogen, oxygen, and nitrogen atoms using electronic ground states of multiple simple compounds that are formed by these elements.[63,64]

RMD treats all atoms in the simulated system as separate interaction centers. However, RMD does not treat electrons explicitly. An instantaneous point charge on each atom is determined by the electrostatic field in the presence of all surrounding charges. An instantaneous valence force and interaction energy between each atom pair are linked to an instantaneous bond order. The latter is a function of an instantaneous bond distance. The bond order concept is used to define other valence interactions, such as bond, lone electron pair, valence angle, conjugation, and torsion angle energies. The pairwise van der Waals energy term describes the short-range electron−electron repulsion, preserving atomic radius, and the longer-range London attractive dispersion. The bond-order cutoff is used to identify molecular species. In this work, the threshold was set to 0.3 for all bond types. Note that definition of a chemical bond is not unique. Different definitions lead to somewhat different reaction intermediates.

The polynitro-CNTs used in the RMD simulations are slightly smaller than those in the NAMD simulations, containing 130 carbon atoms (Figure 1). The model applied is sufficient to capture the mechanism of polynitro-CNT chemical decomposition, because it occurs via local chemical interactions. Furthermore, the RMD simulations used finite size polynitro-CNTs, terminated by hydrogen atoms, because ReaxFF are most easily applied to finite systems.

Following our previous experience on creating the buckybomb,[39] we functionalized (5,0) and (5,5) CNTs with a significant number of $-NO_2$ groups. The ratio between carbon and nitrogen atoms was the same as that in the buckybomb, 5:1. The $-NO_2$ groups were distributed uniformly throughout the external surfaces of CNTs. We ensured that no two $-NO_2$ groups belong to the same six-membered ring of the CNT backbone. Such a structure fosters stability at room conditions and supports rapid decomposition at an elevated temperature.

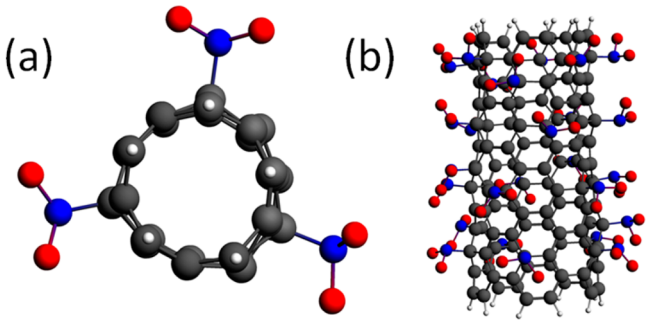

Figure 1. Polynitro-CNTs simulated by RMD: (a) front view of the (5,0) polynitro-CNT; (b) side view of the (5,5) polynitro-CNT. In the front view, a single polynitro-CNT unit cell is depicted for clarity.

Figure 1 depicts initial geometries of the simulated nanostructures, where $-NO_2$ is covalently linked to the CNT backbone.

The reported RMD simulations were performed in the constant energy ensemble (N,V,E) after the systems were heated to 750 K. In experiment, the heating arises due to the electron-vibrational energy redistribution, simulated here by NAMD. In some applications (e.g., medicine), CNTs are surrounded by a solvent or another medium, which can dissipate the heat away from CNTs. The prior studies[20,65,66] have shown that energy transfer from heated CNTs to aqueous and nonaqueous solvents proceeds on fast, subpicosecond and slow, 2−20 ps time scales. It is therefore essential in such cases that a laser is sufficiently intense to deposit significant amounts of energy before it is dissipated into the environment. It should be also noted that heating to temperatures lower than 750 K can also initiate an explosion, with the initiation stage taking longer than in the present simulation. Once the explosion is initiated, it occurs very rapidly, self-supporting itself and generating local temperatures up to 4000 K.

The decomposition took place very quickly, making 100 ps long trajectories sufficient to observe all relevant chemical processes. Due to high-temperature of simulation and therefore large atomic velocities, we used a small time-step of 0.1 fs. Satisfactory conservation of total energy is an important issue in these simulations. The ADF.2013 program, available at https://www.scm.com/, was used to run all RMD calculations. Note that one of the tutorials used involves burning alkanes in the oxygen atmosphere at 3000 K. The process is similar to the phenomena under investigation here.

3. RESULTS AND DISCUSSION

3.1. Charge−Phonon Energy Redistribution. Carrier relaxation dynamics of hot electrons and holes depends strongly on the electronic structure of a system under consideration. The electronic structure of CNTs is characterized by sharp peaks, known as van Hove singularities, superimposed on a continuum background.[67] The singularities are responsible for the strongest light absorption,[68,69] while electron−phonon energy relaxation involves both the singularities and the continuum.[70,71] $-NO_2$ functionalization substantially changes the features of the CNT electronic structure by introducing hybridized states between the singularities.

Figure 2 shows DOS of the pristine and functionalized (5,0) CNT at 0 K. $-NO_2$ groups contribute significantly to the DOS at all energies, including the area near the Fermi energy. Particularly important, the latter fact implies that photoexcitation of the nitro-CNT with near-infrared light will perturb

DOI: 10.1021/jacs.6b08082
J. Am. Chem. Soc. 2016, 138, 15927−15934

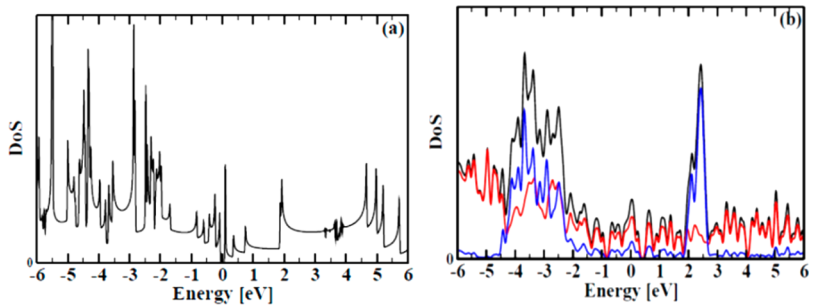

Figure 2. (a) DOS of the pristine (5,0) CNT. (b) Projected DOS of the (5,0) polynitro-CNT. The data are shown for the CNT geometries optimized at 0 K. Zero energy corresponds to the Fermi energy. In (b), the black line represents the total DOS, whereas the red and blue lines represent contributions of the CNT backbone and $-NO_2$ groups, respectively. $-NO_2$ groups contribute substantially to the states near the Fermi level, in both conduction and valence bands.

electronic density localized on the chemically active $-NO_2$ groups. Therefore, the electron−phonon energy relaxation will instantaneously activate these groups. In comparison, if $-NO_2$ groups were not hybridized with the CNT, then their photoexcitation would require energies in the ultraviolet region; consider the sharp rise on the $-NO_2$ partial DOS at +2 eV (Figure 2b).

The effect of $-NO_2$ groups on the CNT electronic properties calculated by the SCC-DFTB method agrees well with the previous results.[72] The nitration has a strong effect on the CNT energy spectrum. The singularities in the DOS of the polynitro-CNT almost vanish, even though the number of nitrogen atoms connected to the CNT backbone is 5 times smaller than the number of carbons in the backbone and no more than one $-NO_2$ group is connected to any six-member carbon ring. The states near the Fermi energy show contributions from both the CNT backbone and $-NO_2$ groups.[72] The Fermi level of the polynitro-CNT shifts toward the valence band. The reduction potential of the $-NO_2$ group is lower than that of the CNT. Therefore, $-NO_2$ accepts electrons from the CNT backbone.[73,74]

The intraband relaxation dynamics of photogenerated hot carriers is investigated for the (5,0) and (5,5) polynitro-CNTs using DFTB-NAMD. The electron and hole relaxation is initiated by excitations of approximately 1 eV away from the Fermi level (Figure 3). The electrons and holes relax nonradiatively to their band edges due to coupling to phonons. The observed energy decay was fitted by the sum of the exponential and Gaussian components, $y = A \times \exp(-(t/\tau)) + (1 - A) \times \exp(-(t/\tau)^2)$. The Gaussian component reflects the initial stages of relaxation, during which only few states are coupled to the initial quantum state. Since the time-derivative of the quantum population is 0 at $t = 0$, Gaussian decayis essential for the quantum Zeno effect.[75] The Gaussian component corresponds to the beginning of the Bloch oscillation of a two-level system. The exponential decay starts once the quantum system has had enough time to explore the Hilbert space and to couple to multiple final states. The electron relaxation in the conduction band takes place within 200 fs in the zigzag (5,0) polynitro-CNT. The magnitude of the Gaussian component $A = 0.33$. The relaxation in the armchair (5,5) polynitro-CNT is slower, 270 fs. Here, $A = 0.13$. In turn, the relaxation of the hole takes 260 fs in the (5,0) polynitro-CNT and 300 fs in the (5,5) polynitro-CNT. The corresponding amplitude fitting parameters are $A = 0.45$ and 0.10. Note that the Gaussian component (A value) is larger for the (5,0) CNT, because it has a lower DOS and hence requires longer time to develop the exponential decay.

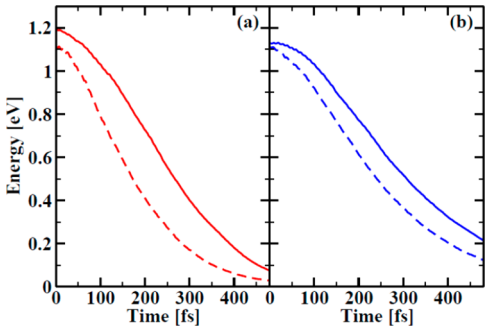

Figure 3. (a) Electron and (b) hole relaxation in the (5,0) and (5,5) polynitro-CNTs, dashed and solid lines, respectively. Electrons decay faster than holes in both CNTs, although DOS is higher for holes (Figure 2). This is because electrons couple to higher frequency phonons (Figure 4).

Holes decay more slowly than electrons in both CNTs. This is surprising, since the DOS of holes is higher than the DOS of electrons. The explanation resides in the phonon modes that facilitate the electron and hole relaxations. The electrons relax faster, because they couple to higher frequency, faster phonons (Figure 4). A similar trend was reported earlier for the (7,0) CNT.[76] The charge−phonon relaxation time scales obtained for the polynitro-CNTs are to those of pristine CNTs, obtained earlier by both experiment[77−79] and theory.[44,76,80−82]

To identify the phonon modes involved in the electron and hole relaxation, Fourier transforms (FT) of the energies of the initial and final states are obtained (Figure 4). The excited electrons interact with high-frequency modes more strongly than holes. This is because electrons are supported by higher energy orbitals, which have more nodes, better matching the finer nodal structure of high-frequency phonons.[76] Thus, the electron relaxation is facilitated by the carbon−carbon stretching longitudinal optical (LO) phonons, around 1500 cm^{-1}.[76,83] The holes relax through the LO modes and the low-frequency breathing modes, <500 cm^{-1}.[76,83] The defect band, 1300 cm^{-1}, indicates the influence of the $-NO_2$ group on the vibrational motion of the polynitro-CNTs.[84] The phonons at 600 and 800 cm^{-1} correspond to the twisting and bending modes[85,86] of $-NO_2$. These modes contribute strongly to the relaxation of electrons and holes. The analysis of the influence spectra (Figure 4) indicates that the electronic excitation energy dissipates nonradiatively through the phonon modes of both the CNT backbone and the $-NO_2$ group.

DOI: 10.1021/jacs.6b08082
J. Am. Chem. Soc. 2016, 138, 15927−15934

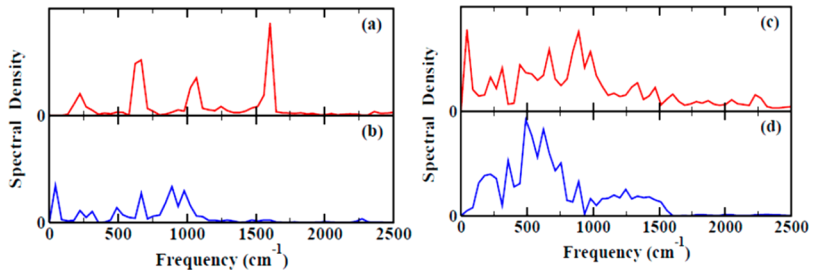

Figure 4. Influence spectra characterizing the phonon modes that couple to electrons and holes in the (5,0) polynitro-CNT. (a and b) Fourier transforms of the dynamics of the initial states of electron and hole. (c and d) Final states of electron and hole. Electron couples to higher frequency phonons than hole. The bands around 1500 cm^{-1} and above are CNT longitudinal optical phonons, including the 1600 cm^{-1} graphene G-band. The band at 1300 cm^{-1} is CNT defect D-band. The $-NO_2$ twisting and bending modes appear at 600 and 800 cm^{-1}, respectively. The low-frequency modes at 500 cm^{-1} and below are CNT breathing modes.

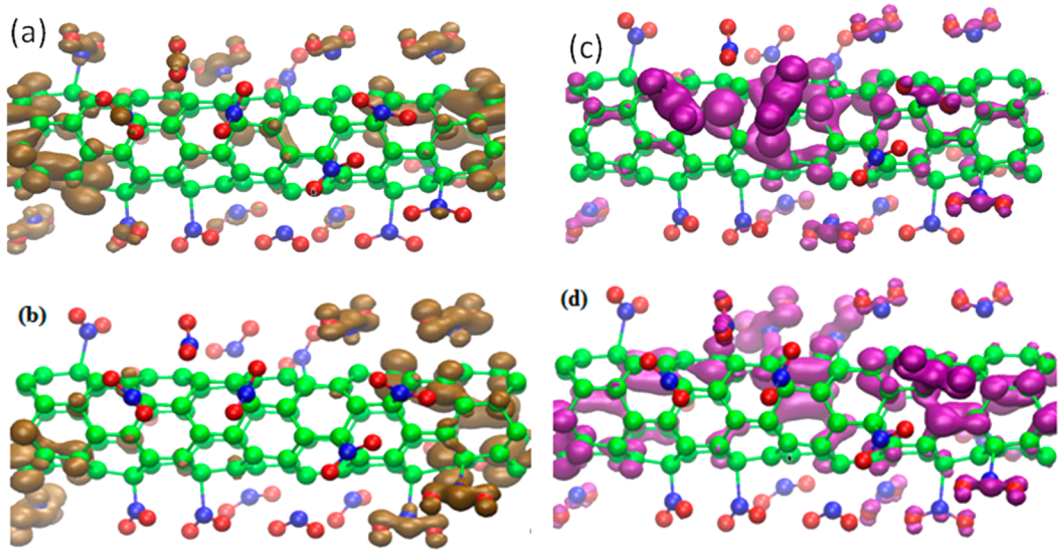

Figure 5. Charge density distributions of (a and c) electron states and (b and d) hole states in the (5,0) polynitro-CNT. (a and b) Initial states of electron and hole; (c and d) final states. The phonon influence spectra for these states are given in Figure 4. Shown are snapshots along a NAMD trajectory.

Charge density distributions in the excited and final states for electrons and holes are provided in Figure 5. The charge density of the $-NO_2$ groups contributes to the total charge density, indicating that $-NO_2$ plays a major role in the electron and hole relaxation of the polynitro-CNTs. This fact is in concordance with the FTs of the energies of the excited and final states of electrons and holes (Figure 4). Indeed, the phonons at 600 and 800 cm^{-1}, corresponding to twisting and bending of $-NO_2$ groups, are prominent in the FTs.

3.2. Explosion of the Nitro-CNTs. Decomposition of the functionalized CNTs begins when the energy of the absorbed photons is redistributed from charges to vibrations. The decomposition process is studied separately by RMD, because it takes 2 orders of magnitude longer than the electron-vibrational energy redistribution and therefore can be regarded as an independent step. Decomposition of the nitrated nanoscale carbon compounds starts with isomerization of the $-NO_2$ group.[39] The first few picoseconds bring liberation of the largest amount of chemical energy, as reflected in the rapid increase of kinetic energy and temperature (Figure 6). Both metallic (5,5) polynitro-CNT and semiconducting (5,0) polynitro-CNT perform in a similar fashion. The temperature growth at the short time is a real physicochemical phenomenon that can be detected, for instance, via changes in frequencies of

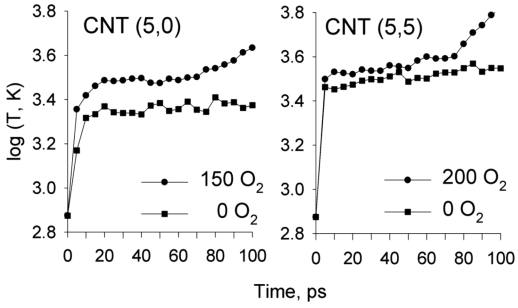

Figure 6. Temperature evolution during explosion of the (5,0) and (5,5) polynitro-CNTs. Following a rapid sub-10 ps jump, the temperature continues to rise at a slower rate. The decomposition is possible with and without oxygen. Oxygen atmosphere facilitates a more complete decomposition and a higher temperature. Generally in a realistic system, the temperature will be decreasing at longer times due to coupling with an environment.

anharmonic vibrations or the effective temperature of the electron Fermi−Dirac distribution, using time-resolved optical measurements. At the same time, the high temperatures produced at the end of the simulations are not realistic, because energy dissipation into environment is not accounted for.

DOI: 10.1021/jacs.6b08082
J. Am. Chem. Soc. 2016, 138, 15927−15934

The decomposition is possible with and without oxygen. The temperature grows more if oxygen is present, because oxygen molecules facilitate more complete decomposition. The difference is more pronounced at longer simulation times. Oxygen is necessary to oxidize numerous carbon atoms of the polynitro-CNTs, transforming them into chemically stable products, such as CO_2. In turn, not all carbon atoms are transformed into gaseous low-molecular-weight products if external oxygen is lacking. Hence, not all available chemical energy is turned into kinetic energy. At the same time, the ability of the polynitro-CNTs to decompose under anaerobic conditions is an important property, which could be particularly beneficial under nanoscale and biological confinement.

Figure 7 presents evolution of selected reactants and products during decomposition of the polynitro-CNTs. The

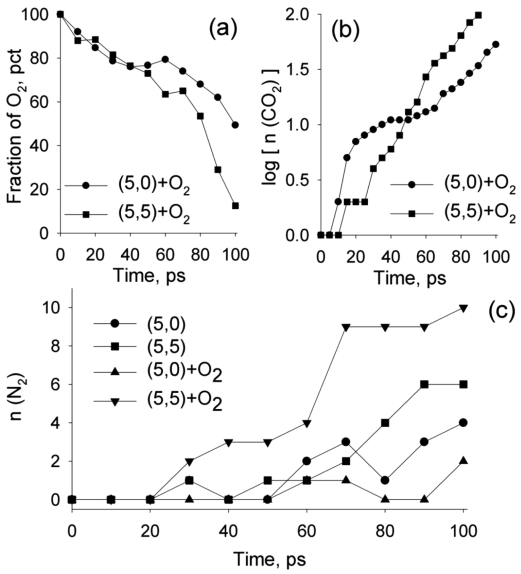

Figure 7. Consumption of oxygen, formation of CO_2, and formation of N_2 during decomposition of the polynitro-CNTs. See legends for line designations; *n* represents the number of moles.

data emphasize the highly nonequilibrium nature of the simulation. The predictions made in Figure 7 can be tested experimentally using pump−probe laser techniques. According to Figure 7 and in line with expectations, CO_2 is the major product (Figure 7b). It is the most thermodynamically stable species formed by oxygen and carbon atoms. Formation of N_2 is strongly dependent on the system composition. The (5,5) polynitro-CNT gives rise to more moles of nitrogen, since more $-NO_2$ groups are available in this molecule. The N_2 molecule is highly stable. For this reason, nitrogen oxides are not observed in these reactions. Water vapor is not formed due to lack of hydrogen atoms.

The explosion process is a rapid liberation of kinetic energy at the expense of potential energy of chemical bonds (Figure 8). There are two major sources of chemical energy in these reactions. The initial energy is released due to isomerization of the $-NO_2$ group into $-O-N-O$. Oxidation of the carbon atoms is the second source of chemical energy. It occurs much slower than the isomerization. Both $-NO_2$ and O_2 species are responsible for the oxidation. The liberated chemical energy amounts to 3−6% of the total initial potential energy of each system, defined in RMD as the binding energy including all covalent bonds. The percentage of the liberated energy is

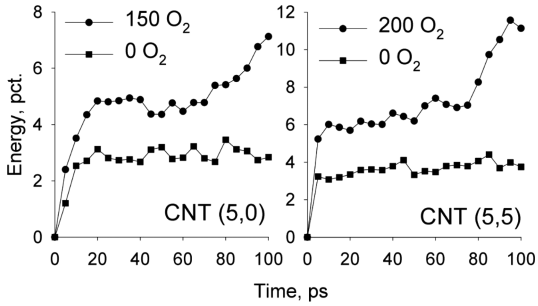

Figure 8. Percentage of energy of covalent bonds released during the decomposition reaction. More energy is released in the presence of O_2. (See Figure 9 for discussion of the data past 80 ps in the O_2-containing systems.)

significantly larger when an excess of molecular oxygen is supplied.

Conservation of the total energy constitutes an important methodological issue in numerical simulations. It is especially important when the results rely on the (N,V,E) ensemble. Energy conservation depends on atomic velocities and integration time-step. Figure 9 investigates this issue. Since

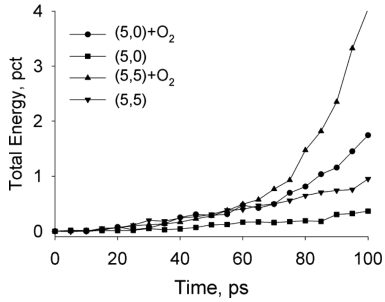

Figure 9. Conservation of the total energy during decomposition of the polynitro-CNTs in the microcanonical ensemble. The 0.1 fs integration time step provides reasonable energy conservation for the duration of the decomposition reaction, with exception of the $(5,5)+O_2$ system past 80 ps.

atomic velocities depend on immediate temperature and temperature increases very significantly during the reaction, the total energy conservation depends on the reaction. Until 80 ps of the simulation, the error falls within 1%, which is an acceptable value. However, it rises appreciably beyond 80 ps in the O_2-containing systems. In comparison, the energies of the polynitro-CNTs decomposing in vacuum are conserved much better. The rapid increase in temperature beyond 80 ps in the O_2-containing systems (Figure 6) is associated with the breakdown of the energy conservation (Figure 9). The accelerated consumption of molecular oxygen (Figure 7a) and the energy growth in the O_2-containing systems (Figure 8) at times beyond 80 ps can be rationalized by the same effect.

4. CONCLUSIONS

We have investigated the physical and chemical processes occurring in the single-walled polynitro-CNTs under an intense laser irradiation. The reported two-step methodology included nonadiabatic MD, employed to understand the nonradiative electron and hole relaxation, and reactive MD, used to observe the decomposition reactions of the excited polynitro-CNTs in real-time. The photogenerated electrons and holes deposit their

DOI: 10.1021/jacs.6b08082
J. Am. Chem. Soc. 2016, 138, 15927−15934

energy into a broad spectrum of phonons within less than a picosecond. Despite a lower density of states, electrons relax more rapidly than holes due to coupling to higher frequency phonons. The orbitals of the nitro-groups mix with the CNT states over a wide energy range, including low energies at which excitation of isolated nitro-groups is not possible. Photo-excitation by a high-energy laser is not required. The electronic energy is deposited immediately to the nitro-groups even if a near-infrared laser suitable for medical applications is used. Rapid delivery of energy to the nitro-groups is important, because decomposition of nitro-CNTs starts by nitro-group isomerization.

The achieved very rapid noninvasive heating of CNTs initiates an explosion, during which the local temperature of polynitro-CNT fragments rises up to several thousand Kelvin. Simple, stable, and nontoxic gas molecules (CO_2, N_2) are formed. The explosion is possible both with and without an external oxygen source. Aerobic explosion is more intense. At the same time, anaerobic explosion is particularly beneficial under biological and nanoscale confinement. The predicted time scales and mechanisms of chemical and physical processes can be tested experimentally using time-resolved pump−probe techniques.

The laser initiated polynitro-CNT decomposition can be important for medical, military, and civil applications. Polynitro-CNTs can be accumulated inside problematic living cells, and their laser-induced decomposition can destroy the cells by generating large amounts of heat. Compared to pristine CNTs, which can transform laser energy into heat, polynitro-CNTs generate much more energy than that provided by the laser, which is only needed to initiate the process. The small CNT size and local laser activation make this procedure significantly less toxic than conventional treatments, such as chemo-therapy. Additionally, CNTs can be used to deliver and release drug molecules. Polynitro-CNT explosives can be activated remotely in military, civil, and industrial applications by a visible or infrared laser, avoiding the need for a detonating cord and improving personnel safety. Our computational results provide a theoretical background for the emerging fields of noninvasive nanomedicine and nanoexplosives.

■ ASSOCIATED CONTENT

Supporting Information

The Supporting Information is available free of charge on the ACS Publications website at DOI: 10.1021/jacs.6b08082.

Parameters file of the force field used in the ReaxFF simulations (TXT)

■ AUTHOR INFORMATION

Corresponding Author

*E-mail: prezhdo@usc.edu.

ORCID

Oleg V. Prezhdo: 0000-0002-5140-7500

Notes

The authors declare no competing financial interest.

■ ACKNOWLEDGMENTS

V.V.C. is CAPES fellow under the "Science Without Borders" program. S.P. and O.V.P. acknowledge financial support of the U.S. Department of Energy, Grant No. DE-SC0014429. O.V.P. is grateful to the Photochemistry Center of the Russian Science Foundation, project No.14-43-00052, for hospitality during manuscript preparation.

■ REFERENCES

(1) Petrosko, S. H.; Johnson, R.; White, H.; Mirkin, C. A. *J. Am. Chem. Soc.* **2016**, *138* (24), 7443−7445.
(2) Abdelhalim, A.; Abdellah, A.; Scarpa, G.; Lugli, P. *Nanotechnology* **2014**, *25* (5), 055208.
(3) Wang, D. Y.; Gong, M.; Chou, H. L.; Pan, C. J.; Chen, H. A.; Wu, Y. P.; Lin, M. C.; Guan, M. Y.; Yang, J.; Chen, C. W.; Wang, Y. L.; Hwang, B. J.; Chen, C. C.; Dai, H. J. *J. Am. Chem. Soc.* **2015**, *137* (4), 1587−1592.
(4) Lu, X. Y.; Yim, W. L.; Suryanto, B. H. R.; Zhao, C. *J. Am. Chem. Soc.* **2015**, *137* (8), 2901−2907.
(5) Chaban, V. V.; Prezhdo, O. V. *ACS Nano* **2014**, *8* (8), 8190−8197.
(6) Fan, Q.; Liu, W.; Weng, Z.; Sun, Y. M.; Wang, H. L. *J. Am. Chem. Soc.* **2015**, *137* (40), 12946−12953.
(7) Choo, H.; Jung, Y.; Jeong, Y.; Kim, H. C.; Ku, B. C. *Carbon Lett.* **2012**, *13* (4), 191−204.
(8) Chen, W.; Fan, Z. L.; Zhang, B.; Ma, G. J.; Takanabe, K.; Zhang, X. X.; Lai, Z. P. *J. Am. Chem. Soc.* **2011**, *133* (38), 14896−14899.
(9) Hu, L. B.; Hecht, D. S.; Gruner, G. *Chem. Rev.* **2010**, *110* (10), 5790−5844.
(10) Musameh, M.; Notivoli, M. R.; Hickey, M.; Kyratzis, I. L.; Gao, Y. A.; Huynh, C.; Hawkins, S. C. *Adv. Mater.* **2011**, *23* (7), 906−910.
(11) Scarselli, M.; Castrucci, P.; De Nicola, F.; Cacciotti, I.; Nanni, F.; Gatto, E.; Venanzi, M.; De Crescenzi, M. *Beilstein J. Nanotechnol.* **2015**, *6*, 792−798.
(12) Chaban, V. *Chem. Phys. Lett.* **2010**, *496* (1−3), 50−55.
(13) Yu, K. H.; Lu, G. H.; Bo, Z.; Mao, S.; Chen, J. H. *J. Phys. Chem. Lett.* **2011**, *2* (13), 1556−1562.
(14) Xiao, J. P.; Pan, X. L.; Guo, S. J.; Ren, P. J.; Bao, X. H. *J. Am. Chem. Soc.* **2015**, *137* (1), 477−482.
(15) Murakami, T.; Nakatsuji, H.; Inada, M.; Matoba, Y.; Umeyama, T.; Tsujimoto, M.; Isoda, S.; Hashida, M.; Imahori, H. *J. Am. Chem. Soc.* **2012**, *134* (43), 17862−17865.
(16) Liu, Z.; Sun, X. M.; Nakayama-Ratchford, N.; Dai, H. J. *ACS Nano* **2007**, *1* (1), 50−56.
(17) Chaban, V. V.; Prezhdo, O. V. *ACS Nano* **2011**, *5* (7), 5647−5655.
(18) Zhao, Y.; Burkert, S. C.; Tang, Y. F.; Sorescu, D. C.; Kapralov, A. A.; Shurin, G. V.; Shurin, M. R.; Kagan, V. E.; Star, A. *J. Am. Chem. Soc.* **2015**, *137* (2), 675−684.
(19) Wang, X. J.; Wang, C.; Cheng, L.; Lee, S. T.; Liu, Z. *J. Am. Chem. Soc.* **2012**, *134* (17), 7414−7422.
(20) Chaban, V. V.; Savchenko, T. I.; Kovalenko, S. M.; Prezhdo, O. V. *J. Phys. Chem. B* **2010**, *114* (42), 13481−13486.
(21) Lucente-Schultz, R. M.; Moore, V. C.; Leonard, A. D.; Price, B. K.; Kosynkin, D. V.; Lu, M.; Partha, R.; Conyers, J. L.; Tour, J. M. *J. Am. Chem. Soc.* **2009**, *131* (11), 3934−3941.
(22) Pantarotto, D.; Partidos, C. D.; Graff, R.; Hoebeke, J.; Briand, J. P.; Prato, M.; Bianco, A. *J. Am. Chem. Soc.* **2003**, *125* (20), 6160−6164.
(23) Su, Z. D.; Zhu, S. H.; Donkor, A. D.; Tzoganakis, C.; Honek, J. F. *J. Am. Chem. Soc.* **2011**, *133* (18), 6874−6877.
(24) Soleyman, R.; Hirbod, S.; Adeli, M. *Biomater. Sci.* **2015**, *3* (5), 695−711.
(25) Reza, K. K.; Srivastava, S.; Yadav, S. K.; Biradar, A. M. *Mater. Lett.* **2014**, *126*, 126−130.
(26) Wang, W.; Zhu, Y. H.; Liao, S. S.; Li, J. J. *BioMed Res. Int.* **2014**, *2014*, 518609.
(27) Myers, T. W.; Bjorgaard, J. A.; Brown, K. E.; Chavez, D. E.; Hanson, S. K.; Scharff, R. J.; Tretiak, S.; Veauthier, J. M. *J. Am. Chem. Soc.* **2016**, *138* (13), 4685−4692.
(28) Zhou, X.; Torabi, M.; Lu, J.; Shen, R.; Zhang, K. *ACS Appl. Mater. Interfaces* **2014**, *6* (5), 3058−3074.
(29) Li, C. W.; Ciston, J.; Kanan, M. W. *Nature* **2014**, *508* (7497), 504−507.

DOI: 10.1021/jacs.6b08082
J. Am. Chem. Soc. 2016, 138, 15927−15934

(30) Mehrkesh, A.; Karunanithi, A. T. *ACS Sustainable Chem. Eng.* **2013**, *1* (4), 448−455.
(31) Yu, T.-Q.; Tuckerman, M. E. *Phys. Rev. Lett.* **2011**, *107* (1), 015701.
(32) Greenfield, M. T.; McGrane, S. D.; Bolme, C. A.; Bjorgaard, J. A.; Nelson, T. R.; Tretiak, S.; Scharff, R. J. *J. Phys. Chem. A* **2015**, *119* (20), 4846−4855.
(33) Song, M. Y.; Zeng, L. Z.; Yuan, S. P.; Yin, J. F.; Wang, H. L.; Jiang, G. B. *Chemosphere* **2013**, *92* (5), 576−582.
(34) Bonafe, R.; Bardini, P.; Bussi, S.; Maiocchi, A. *Toxicol. Lett.* **2008**, *180*, S220−S221.
(35) Zavaleta, C.; de la Zerda, A.; Liu, Z.; Keren, S.; Cheng, Z.; Schipper, M.; Chen, X.; Dai, H.; Gambhir, S. S. *Nano Lett.* **2008**, *8* (9), 2800−2805.
(36) Fileti, E. E.; Chaban, V. V.; Prezhdo, O. V. *J. Phys. Chem. Lett.* **2014**, *5* (19), 3415−3420.
(37) Michinobu, T.; Okoshi, K.; Murakami, Y.; Shigehara, K.; Ariga, K.; Nakanishi, T. *Langmuir* **2013**, *29* (17), 5337−44.
(38) Assali, M.; Cid, J. J.; Pernia-Leal, M.; Munoz-Bravo, M.; Fernandez, I.; Wellinger, R. E.; Khiar, N. *ACS Nano* **2013**, *7* (3), 2145−53.
(39) Chaban, V. V.; Fileti, E. E.; Prezhdo, O. V. *J. Phys. Chem. Lett.* **2015**, *6* (5), 913−917.
(40) Cataldo, F.; Ursini, O.; Angelini, G. *Carbon* **2013**, *62*, 413−421.
(41) Wang, N.-X. *Propellants, Explos., Pyrotech.* **2001**, *26*, 109−111.
(42) Chaban, V. V.; Fileti, E. E.; Prezhdo, O. V. *J. Phys. Chem. Lett.* **2015**, *6* (5), 913−917.
(43) Fecht, H. J., Brühne, K., Eds. *Carbon-Based Nanomaterials and Hybrids: Synthesis, Properties, and Commercial Applications*; CRC Press: Boca Raton, FL, 2014; p 220.
(44) Pal, S.; Trivedi, D. J.; Akimov, A. V.; Aradi, B.; Frauenheim, T.; Prezhdo, O. V. *J. Chem. Theory Comput.* **2016**, *12*, 1436−1448.
(45) Aradi, B.; Hourahine, B.; Frauenheim, T. *J. Phys. Chem. A* **2007**, *111* (26), 5678−5684.
(46) Elstner, M. *J. Phys. Chem. A* **2007**, *111* (26), 5614−5621.
(47) Elstner, M.; Porezag, D.; Jungnickel, G.; Elsner, J.; Haugk, M.; Frauenheim, T.; Suhai, S.; Seifert, G. *Phys. Rev. B: Condens. Matter Mater. Phys.* **1998**, *58* (11), 7260.
(48) Krüger, T.; Elstner, M.; Schiffels, P.; Frauenheim, T. *J. Chem. Phys.* **2005**, *122* (11), 114110.
(49) Niehaus, T. A.; Suhai, S.; Della Sala, F.; Lugli, P.; Elstner, M.; Seifert, G.; Frauenheim, T. *Phys. Rev. B: Condens. Matter Mater. Phys.* **2001**, *63* (8), 085108.
(50) Porezag, D.; Frauenheim, T.; Köhler, T.; Seifert, G.; Kaschner, R. *Phys. Rev. B: Condens. Matter Mater. Phys.* **1995**, *51* (19), 12947.
(51) Seifert, G. *J. Phys. Chem. A* **2007**, *111* (26), 5609−5613.
(52) Kohn, W.; Sham, L. J. *Phys. Rev.* **1965**, *140* (4A), A1133.
(53) Craig, C. F.; Duncan, W. R.; Prezhdo, O. V. *Phys. Rev. Lett.* **2005**, *95* (16), 163001.
(54) Fischer, S. A.; Habenicht, B. F.; Madrid, A. B.; Duncan, W. R.; Prezhdo, O. V. *J. Chem. Phys.* **2011**, *134* (2), 024102.
(55) Tully, J. C. *J. Chem. Phys.* **1990**, *93* (2), 1061−1071.
(56) Parandekar, P. V.; Tully, J. C. *J. Chem. Phys.* **2005**, *122* (9), 094102.
(57) Akimov, A. V.; Prezhdo, O. V. *J. Chem. Theory Comput.* **2013**, *9* (11), 4959−4972.
(58) Akimov, A. V.; Prezhdo, O. V. *J. Chem. Theory Comput.* **2014**, *10* (2), 789−804.
(59) Zheng, J. J.; Meana-Paneda, R.; Truhlar, D. G. *J. Phys. Chem. Lett.* **2014**, *5* (11), 2039−2043.
(60) Frauenheim, T.; Seifert, G.; Elstner, M.; Niehaus, T.; Köhler, C.; Amkreutz, M.; Sternberg, M.; Hajnal, Z.; Di Carlo, A.; Suhai, S. *J. Phys.: Condens. Matter* **2002**, *14* (11), 3015.
(61) Monkhorst, H. J.; Pack, J. D. *Phys. Rev. B* **1976**, *13* (12), 5188.
(62) Verlet, L. *Phys. Rev.* **1967**, *159* (1), 98−103.
(63) Chenoweth, K.; van Duin, A. C. T.; Goddard, W. A. *J. Phys. Chem. A* **2008**, *112* (5), 1040−1053.
(64) Weismiller, M. R.; van Duin, A. C. T.; Lee, J.; Yetter, R. A. *J. Phys. Chem. A* **2010**, *114* (17), 5485−5492.
(65) Nelson, T. R.; Chaban, V. V.; Kalugin, O. N.; Prezhdo, O. V. *J. Phys. Chem. B* **2010**, *114* (13), 4609−4614.
(66) Nelson, T. R.; Chaban, V. V.; Prezhdo, V. V.; Prezhdo, O. V. *J. Phys. Chem. B* **2011**, *115* (18), 5260−5267.
(67) Saito, R.; Dresselhaus, G.; Dresselhaus, M. S. *Physical properties of carbon nanotubes*; Imperial College Press: London, 1998; Vol. 35.
(68) Bachilo, S. M.; Strano, M. S.; Kittrell, C.; Hauge, R. H.; Smalley, R. E.; Weisman, R. B. *Science* **2002**, *298* (5602), 2361−2366.
(69) Weisman, R. B.; Bachilo, S. M. *Nano Lett.* **2003**, *3* (9), 1235−1238.
(70) Postupna, O.; Jaeger, H. M.; Prezhdo, O. V. *J. Phys. Chem. Lett.* **2014**, *5* (21), 3872−3877.
(71) Postupna, O.; Long, R.; Prezhdo, O. V. *J. Phys. Chem. C* **2015**, *119* (21), 12088−12094.
(72) Chang, H.; Lee, J.; Lee, S.; Lee, Y. H. *Appl. Phys. Lett.* **2001**, *79* (23), 3863−3865.
(73) Kong, J.; Franklin, N. R.; Zhou, C.; Chapline, M. G.; Peng, S.; Cho, K.; Dai, H. *Science* **2000**, *287* (5453), 622−625.
(74) Seo, K.; Park, K. A.; Kim, C.; Han, S.; Kim, B.; Lee, Y. H. *J. Am. Chem. Soc.* **2005**, *127* (45), 15724−15729.
(75) Kilina, S. V.; Neukirch, A. J.; Habenicht, B. F.; Kilin, D. S.; Prezhdo, O. V. *Phys. Rev. Lett.* **2013**, *110* (18), 180404.
(76) Habenicht, B. F.; Craig, C. F.; Prezhdo, O. V. *Phys. Rev. Lett.* **2006**, *96* (18), 187401.
(77) Hertel, T.; Moos, G. *Phys. Rev. Lett.* **2000**, *84* (21), 5002−5005.
(78) Korovyanko, O. J.; Sheng, C. X.; Vardeny, Z. V.; Dalton, A. B.; Baughman, R. H. *Phys. Rev. Lett.* **2004**, *92* (1), 017403.
(79) Manzoni, C.; Gambetta, A.; Menna, E.; Meneghetti, M.; Lanzani, G.; Cerullo, G. *Phys. Rev. Lett.* **2005**, *94* (20), 207401.
(80) Habenicht, B. F.; Prezhdo, O. V. *J. Phys. Chem. C* **2009**, *113* (32), 14067−14070.
(81) Long, R.; Prezhdo, O. V. *Nano Lett.* **2014**, *14* (6), 3335−3341.
(82) Habenicht, B. F.; Prezhdo, O. V. *Phys. Rev. Lett.* **2008**, *100* (19), 197402.
(83) Kilina, S.; Habenicht, B. F. *Excitonic and Vibrational Dynamics in Nanotechnology*; Pan Stanford Publishing: Singapore, 2009.
(84) Anderson, N.; Hartschuh, A.; Cronin, S.; Novotny, L. *J. Am. Chem. Soc.* **2005**, *127* (8), 2533−2537.
(85) Song, Y.; Hemley, R. J.; Liu, Z.; Somayazulu, M.; Mao, H.-k.; Herschbach, D. R. *J. Chem. Phys.* **2003**, *119* (4), 2232.
(86) Ellison, M. D.; Crotty, M. J.; Koh, D.; Spray, R. L.; Tate, K. E. *J. Phys. Chem. B* **2004**, *108* (23), 7938−7943.

DOI: 10.1021/jacs.6b08082
J. Am. Chem. Soc. 2016, 138, 15927−15934